Spin-filter effect and spin-polarized optoelectronic properties in annulene-based molecular spintronic devices*

Zhiyuan Ma(马志远)[1], Ying Li(李莹)[1], Xian-Jiang Song(宋贤江)[1], Zhi Yang(杨致)[1,†], Li-Chun Xu(徐利春)[1], Ruiping Liu(刘瑞萍)[1], Xuguang Liu(刘旭光)[2,3], and Dianyin Hu(胡殿印)[4,5]

[1] *College of Physics and Optoelectronics, Taiyuan University of Technology, Taiyuan* 030024, *China*
[2] *Key Laboratory of Interface Science and Engineering in Advanced Materials, Ministry of Education, Taiyuan University of Technology, Taiyuan* 030024, *China*
[3] *College of Chemistry and Chemical Engineering, Taiyuan University of Technology, Taiyuan* 030024, *China*
[4] *School of Energy and Power Engineering, Beihang University, Beijing* 100191, *China*
[5] *Beijing Key Laboratory of Aero-Engine Structure and Strength, Beijing* 100191, *China*

(Received 16 November 2016; revised manuscript received 17 March 2017; published online 20 April 2017)

Using Fe, Co or Ni chains as electrodes, we designed several annulene-based molecular spintronic devices and investigated the quantum transport properties based on density functional theory and non-equilibrium Green's function method. Our results show that these devices have outstanding spin-filter capabilities and exhibit giant magnetoresistance effect, and that with Ni chains as electrodes, the device has the best transport properties. Furthermore, we investigated the spin-polarized optoelectronic properties of the device with Ni electrodes and found that the spin-polarized photocurrents can be directly generated by irradiating the device with infrared, visible or ultraviolet light. More importantly, if the magnetization directions of the two electrodes are antiparallel, the photocurrents with different spins are spatially separated, appearing at different electrodes. This phenomenon provides a new way to simultaneously generate two spin currents.

Keywords: annulene molecular, molecular spintronic devices, quantum transport properties

PACS: 72.10.–d, 72.10.Fk, 05.60.Gg **DOI:** 10.1088/1674-1056/26/6/067201

1. Introduction

Molecular spintronics, which offers new possibilities for continuing the miniaturization of electronic devices beyond the limits of traditional technologies,[1–10] has attracted great attention in recent years. By manipulating charges and spins in molecular spintronic devices, many interesting and novel phenomena, e.g., spin valve,[11] spin filter,[12,13] Kondo effect,[14] and spin crossover,[15,16] have been observed. Molecular spintronics is a rich field which promises scientific and technological breakthroughs.

Compared with conventional metals and semiconductors, organic molecules have weaker spin–orbit and hyperfine interactions, leading to longer spin-coherence time and distance. Therefore, organic molecules are powerful candidates for constructing molecular spintronic devices.[17–31] For example, in a recent experiment Petta *et al.* studied the spin-dependent transport of electrons in the octanethiol-based molecular tunnel junctions.[22] In another experiment, Schmaus and the coworkers measured the giant magnetoresistance of a phthalocyanine molecule.[23]

In addition to the experimental discoveries, theoretical studies have made progress as well.[24–27,27,29–31] For instance, using density functional theory, Pati *et al.* investigated the spin-polarized transport properties of electrons in a benzene-1-4-dithiolate molecule which is sandwiched between two Ni layers.[26] Chen and coworkers reported a theoretical study of the charge and spin transport of a chromium porphyrin-based molecular device.[27] In fact, previous studies have shown that, to effectively transmit charge or spin, the better choice for designing molecular spintronic devices is π-conjugated systems such as graphene or benzene,[26,31] since in these systems π electrons are delocalized, resulting in sensitive and interesting transport properties.

Annulenes are a kind of fascinating organic molecules since they hold distinctive geometric structures and fantastic electronic properties. As the smallest annulene, 1,6-methano-(10)-annulene has been successfully synthesized in many different experiments.[32,33] 1,6-methano-(10)-annulene is a stable π-conjugated molecule and has significant aromatic feature. In addition, the molecule has C_{2v} symmetry and the methylene bridge maintains the planarity of annulene, which is the origination of the aromaticity. Because the molecule has delocalized electrons, its derivatives have a wide range

*Project supported by the National Natural Science Foundation of China (Grant Nos. U1510132, U1610255, 51401142, and 11604235), the Key Innovative Research Team in Science and Technology of Shanxi Province, China (Grant No. 201605D131045-10), the Natural Science Foundation of Shanxi Province, China (Grant Nos. 2015021027 and 2016021030), the Scientific and Technological Innovation Program of the Higher Education Institutions of Shanxi Province, China (Grant No. 2016140), and the Program for the Outstanding Innovative Teams of the Higher Learning Institutions of Shanxi Province, China.

†Corresponding author. E-mail: yangzhi@tyut.edu.cn

© 2017 Chinese Physical Society and IOP Publishing Ltd

of applications in different fields such as electronic luminous materials.[34] Although the chemical properties of the annulenes have been widely investigated,[35,36] to our knowledge, the transport properties are still open questions.

In the present study, using 1,6-methano-(10)-annulene as an example, we theoretically designed and explored several different molecular spintronic devices. Our results show that, using Fe, Co or Ni chains as electrodes, under finite bias voltages the devices can exhibit significant giant magnetoresistance effect and high spin-filter capability. With Ni chains as the electrodes, the device has the best transport properties. In addition, the spin-polarized optoelectronic properties of the device with Ni electrodes were further investigated. We found that the spin-polarized photocurrents can be directly generated in the device.

2. Models and computational details

The designed molecular spintronic device is shown in Fig. 1(a). The whole device is divided into three parts, namely, the left electrode, the central region and the right electrode. To consider the influence of the electrode materials, three transition-metal (TM = Fe, Co or Ni) chains are used as the magnetic electrodes. The TM chains have been successfully employed as magnetic electrodes for different molecular spintronic devices in previous studies.[11,37] Furthermore, in order to effectively enhance the connection between the molecule and the chain, like previous treatments,[38,39] two S atoms are introduced in the system.

The schematic plots of the device are presented in Fig. 1(b). The magnetization directions of the two electrodes could be parallel (P) or antiparallel (AP). For P and AP spin configurations, the transport properties of the device are different. Therefore, the notations M_{TM}, M_{TM_P}, and M_{TM_AP} are employed to distinguish the devices with different electrodes and spin configurations. For example, M_{Fe} indicates that the electrodes of the device are Fe chains, while M_{Fe_P} (M_{Fe_AP}) further shows that the magnetic moments of the two Fe chains are parallel (antiparallel).

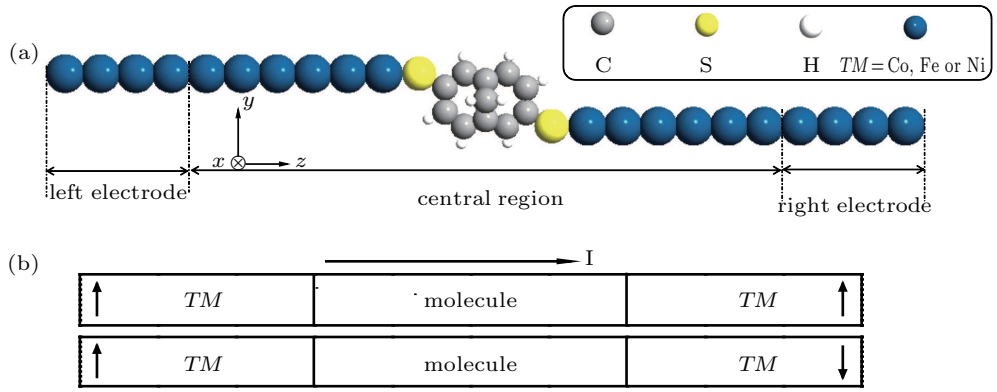


Fig. 1. (color online) (a) The designed annulene-based molecular spintronic device. In the device the annulene molecule is connected to the TM chain by S atoms. Here, three TM chains are used as electrodes (TM = Fe, Co or Ni). (b) The schematic plots of the device. The arrows represent the magnetization directions of the electrodes while I is the total current through the device.

The structures of devices were firstly optimized by using density functional theory (DFT) as implemented in Atomistix ToolKit (ATK) package.[40] The exchange-correlation functional was treated within the generalized gradient approximation proposed by Perdew, Burke and Ernzerhof (PBE),[41] and the double-ζ plus polarization (DZP) basis sets were adopted in the calculation. The spin-dependent transport properties of the devices were then studied by the combination of DFT and non-equilibrium Green's function (NEGF) method.[42,43]

Careful and extensive convergence tests were performed. Finally, the kinetic cutoff energy was set to 200 Ry (1 Ry = 13.6056923 eV) and, during the optimization, a criterion of 0.01 eV/Å for atomic force was employed. The Brillouin zone was sampled by $1 \times 1 \times 100$ mesh points in the k-space. Since the transport is along z axis, in x and y directions large vacuum space was included in the supercell to avoid the interactions between the periodic images.

The spin current I_σ as a function of bias voltage V_b can be calculated from Landauer-like formula:[44]

$$I_\sigma(V_b) = (e/h)\int T_\sigma(E,V_b)[f_L(E) - f_R(E)]\mathrm{d}E, \qquad (1)$$

where $\sigma = \uparrow$ (spin up) and $\downarrow$ (spin down), e is the electron charge, h is the Planck's constant, $T_\sigma(E,V_b)$ is the bias-dependent transmission coefficient and $f_{L(R)}(E)$ is the Fermi–Dirac distribution of the left (right) electrode. The total current under P or AP spin configurations is defined as

$$I^P = I^P_\uparrow + I^P_\downarrow \quad \text{or} \quad I^{AP} = I^{AP}_\uparrow + I^{AP}_\downarrow, \qquad (2)$$

where I^P_σ and I^{AP}_σ are the corresponding spin currents calculated from Eq. (1). In addition, the total transmission coefficients could be expressed as

$$T^P(E) = T^P_\uparrow(E) + T^P_\downarrow(E) \quad \text{or}$$

$$T^{\mathrm{AP}}(E) = T^{\mathrm{AP}}_{\uparrow}(E) + T^{\mathrm{AP}}_{\downarrow}(E). \quad (3)$$

The giant magnetoresistance (GMR) is defined as

$$\mathrm{GMR} = [T^{\mathrm{P}}(E_{\mathrm{F}}) - T^{\mathrm{AP}}(E_{\mathrm{F}})]/T^{\mathrm{AP}}(E_{\mathrm{F}}) \quad (V_{\mathrm{b}} = 0\ \mathrm{V})$$

or

$$\mathrm{GMR} = (I^{\mathrm{P}} - I^{\mathrm{AP}})/I^{\mathrm{AP}} \quad (V_{\mathrm{b}} \neq 0\ \mathrm{V}), \quad (4)$$

where E_{F} is the Fermi level. The spin filter efficiency (SFE) of current under P configuration can be calculated from

$$\mathrm{SFE}^{\mathrm{P}} = [T^{\mathrm{P}}_{\uparrow}(E_{\mathrm{F}}) - T^{\mathrm{P}}_{\downarrow}(E_{\mathrm{F}})]/[T^{\mathrm{P}}_{\uparrow}(E_{\mathrm{F}}) + T^{\mathrm{P}}_{\downarrow}(E_{\mathrm{F}})] \quad (V_{\mathrm{b}} = 0\ \mathrm{V})$$

or

$$\mathrm{SFE}^{\mathrm{P}} = (I^{\mathrm{P}}_{\uparrow} - I^{\mathrm{P}}_{\downarrow})/(I^{\mathrm{P}}_{\uparrow} + I^{\mathrm{P}}_{\downarrow}) \quad (V_{\mathrm{b}} \neq 0\ \mathrm{V}). \quad (5)$$

As we will see later, under AP configuration for all the devices the spin current I^{AP}_{σ} is close to zero, thus here we mainly focus on $\mathrm{SFE}^{\mathrm{P}}$.

Using Nanodcal package,[45] at the same theoretical level (PBE/DZP), we calculated the linear photocurrent I_{ph} from:[46]

$$I_{\mathrm{ph}} = \mathrm{i}e/2h \int \mathrm{Tr}\{[\Gamma^{\mathrm{L}}(E) - \Gamma^{\mathrm{R}}(E)]G^{<}(E) + [f_{\mathrm{L}}(E)\Gamma^{\mathrm{L}}(E) - f_{\mathrm{R}}(E)\Gamma^{\mathrm{R}}(E)] \times [G^{\mathrm{r}}(E) - G^{\mathrm{a}}(E)]\}\,\mathrm{d}E, \quad (6)$$

where $\Gamma^{\mathrm{L(R)}}(E)$ is the self-energy function, representing the coupling between the central scattering region and the left (right) electrode, $G^{<}(E)$ is the lesser Green's function and $G^{\mathrm{r(a)}}(E)$ is the retarded (advanced) Green's function. It is easy to check that I_{ph} is proportional to the photon flux. Accordingly, we can define the photoresponse function R as

$$R = I_{\mathrm{ph}}/eF, \quad (7)$$

where F is the photon flux. Like Eq. (2), the R function can be further written as

$$R^{\mathrm{P}} = R^{\mathrm{P}}_{\uparrow} + R^{\mathrm{P}}_{\downarrow} \quad \text{or} \quad R^{\mathrm{AP}} = R^{\mathrm{AP}}_{\uparrow} + R^{\mathrm{AP}}_{\downarrow}, \quad (8)$$

where R^{P}_{σ} and R^{AP}_{σ} represent spin photoresponse functions.

3. Results and discussion

3.1. The transport properties of the devices under finite bias voltage

To verify the spin configurations of the devices, the spin difference densities are plotted in Fig. 2. The spin difference density represents the distribution of unpaired electrons in the system.[47] For the three devices, it is obvious that all the TM atoms have large magnetic moments, and that in AP case the spins of the two electrodes are opposite. In addition, the connection of the S atom and TM chain destroys the spin degeneracy, leading to a very small induced magnetic moment on the S atom. As to the annulene molecule, the net spin density is nearly zero and the magnetic moment can be ignored for the two spin configurations.

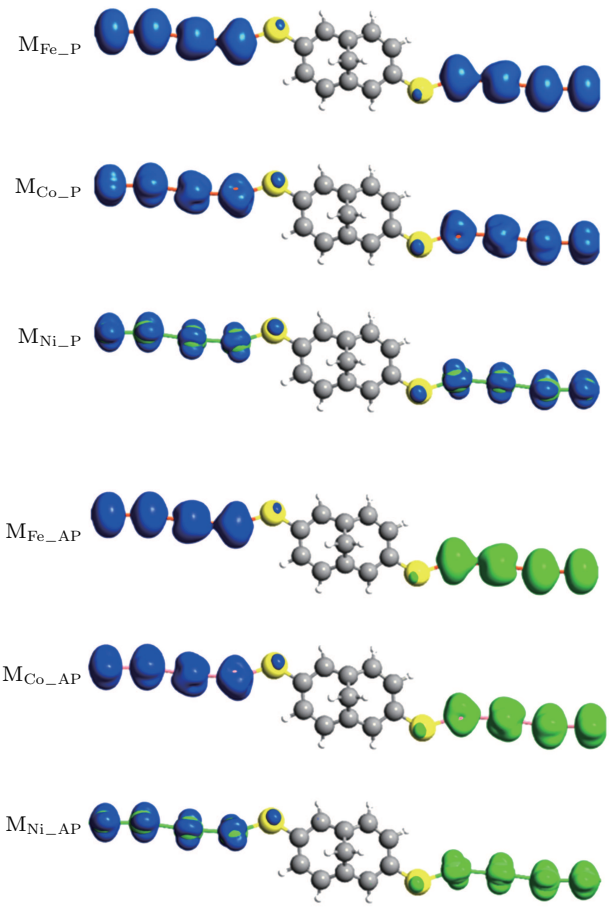


Fig. 2. (color online) The spin difference densities of $\mathrm{M}_{TM_\mathrm{P}}$ and $\mathrm{M}_{TM_\mathrm{AP}}$ (TM = Fe, Co or Ni). The values for blue and green isosurfaces are ±0.005 e/Å^3, respectively.

The total and spin currents of the devices are given in Fig. 3. Interestingly, although the electrode materials of the three devices are different, the trends of the current–voltage curves are similar. We see that, for the P and AP spin configurations, the I^{P} and I^{AP} curves exhibit different behaviors. Generally speaking, I^{P} increases with V_{b} while I^{AP} is always close to zero in the whole bias range. In particular, for M_{Ni}, its I^{P} rapidly increases from 0 to about 9.0 μA. The phenomenon implies that the magnetoresistance of the device should be outstanding. Indeed, as can be seen from Fig. 4(a), the GMR of M_{Ni} is largest, close to 10^4%, and is larger than those of porphyrin-based and Fe_4-based molecular spintronic devices.[48,49] In addition, the significant GMR effect in M_{Fe} and M_{Co} still exists and the GMR values of the two devices are very close.

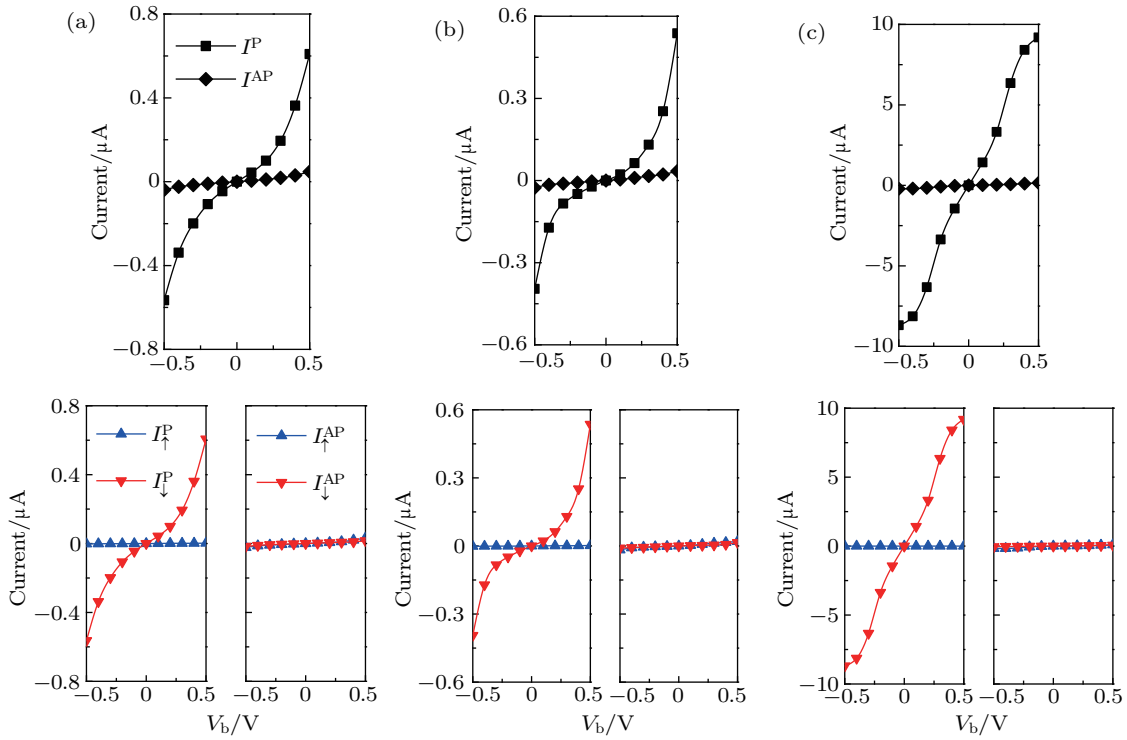


Fig. 3. (color online) The total currents and spin currents of the devices (a) M_{Fe}, (b) M_{Co}, and (c) M_{Ni}.

For the P spin configuration, the spin currents $I^{\rm P}_{\uparrow}$ and $I^{\rm P}_{\downarrow}$ are different. From Fig. 3, we see that the spin-up currents of all the devices are nearly zero, i.e., $I^{\rm P}_{\uparrow} \approx 0$ μA. Therefore, there are no spin-up transport channels opened around the Fermi level and the related spin current is suppressed. In contrast, the spin-down current $I^{\rm P}_{\downarrow}$ increases rapidly with $V_{\rm b}$, finally resulting in $I^{\rm P} = I^{\rm P}_{\uparrow} + I^{\rm P}_{\downarrow} \approx I^{\rm P}_{\downarrow}$. This phenomenon is particularly interesting since it suggests that these devices can be used as perfect spin filters.[50–52] This is confirmed by calculating $\rm SFE^P$. As can be seen from Fig. 4(b), for all the three devices, their $\rm SFE^P$ values are higher than −95% and, more importantly, nearly −100% spin-filter capability is observed in M_{Ni} in the whole bias range. For comparison, we further calculated the $\rm SFE^P$ value of the perfect Ni chain at zero-bias voltage. Our results show that for the Ni chain, the $\rm SFE^P$ is about −71.42%, which is lower than the result of annulene-based device. Therefore, the spin-filter capability of the device is enhanced. In a word, outstanding magnetoresistance and excellent spin-filter capability suggest that M_{Ni} has the best transport properties and may be used as a multifunctional device. As to the AP spin configuration, the calculated results show that for all the devices $I^{\rm AP}_{\uparrow} \approx I^{\rm AP}_{\downarrow} \approx 0$ μA, thus it is not surprising that $I^{\rm AP} = I^{\rm AP}_{\uparrow} + I^{\rm AP}_{\downarrow} \approx 0$ μA. To understand the mechanism of the spin-dependent transport in the systems, we calculated the spin-resolved transmission spectrum and local device density of states (LDDOS). Since the current curves under $V_{\rm b}$ and $-V_{\rm b}$ are similar, as examples, only the transmission spectra under positive bias voltages are shown in Fig. 5. It is obvious that the transmission spectra for the P and AP spin configurations have different behaviors, indicating that the electron transport process depends on the magnetization directions of the electrodes.

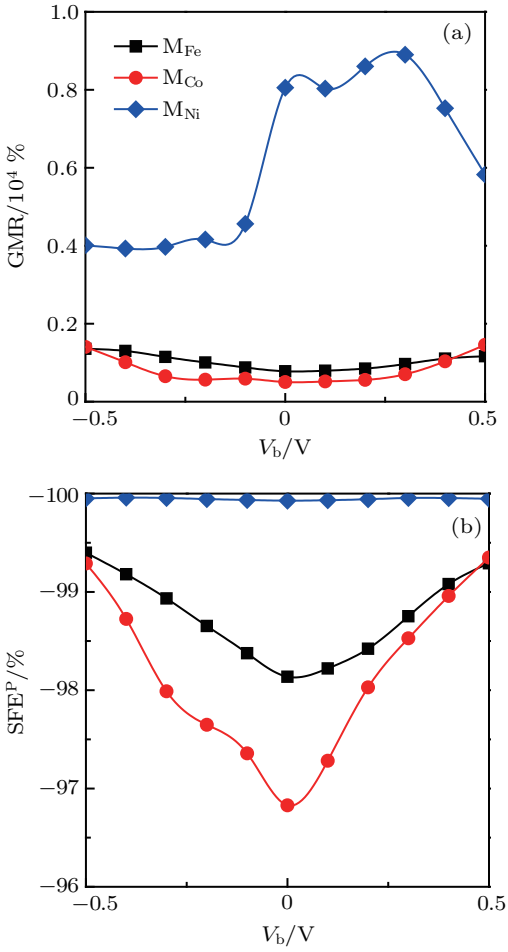


Fig. 4. (color online) (a) The GMR and (b) the $\rm SFE^P$ curves of the M_{TM} (TM = Fe, Co or Ni).

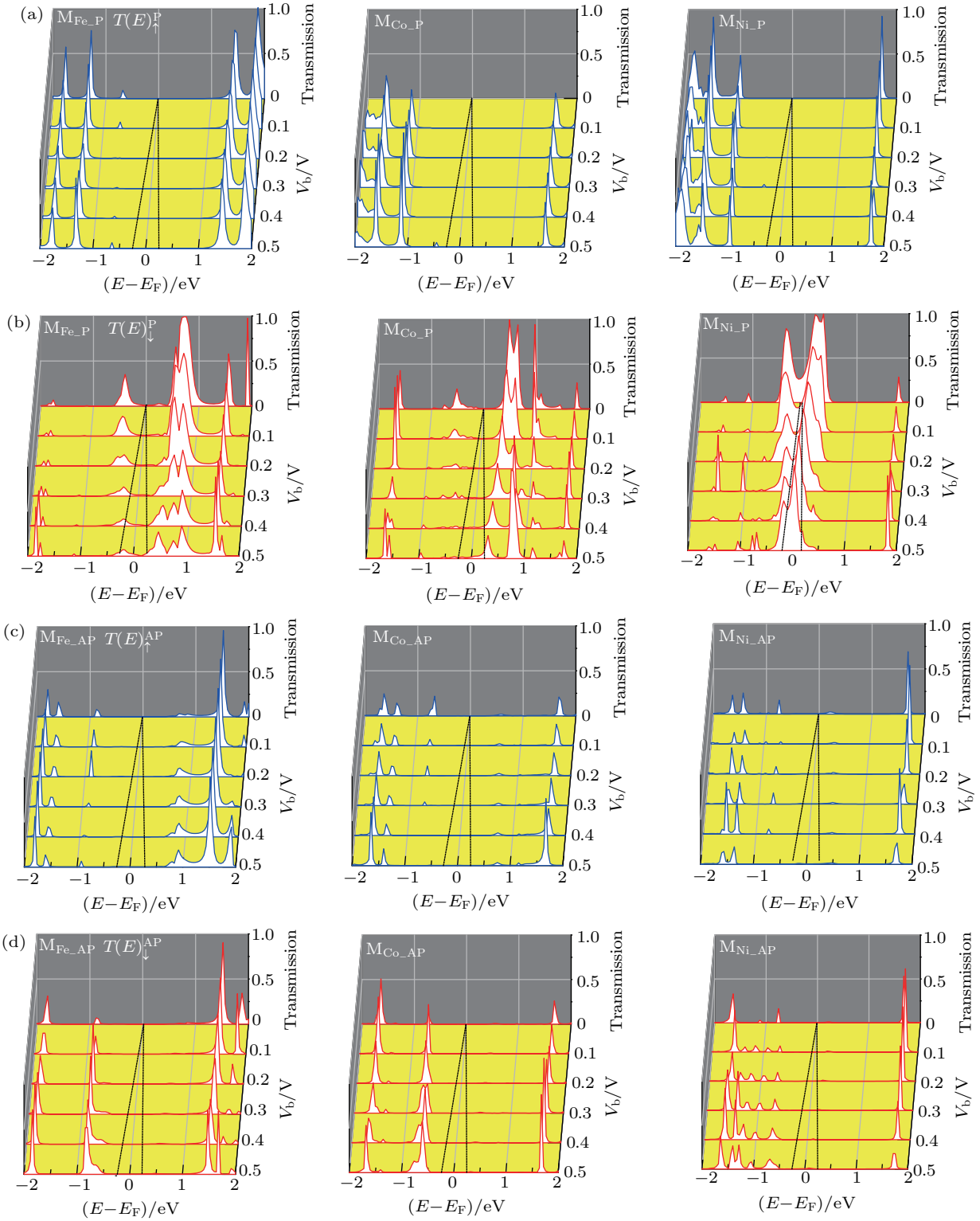


Fig. 5. (color online) The spin-resolved transmission spectra of (a) and (b) M_{TM_P}, (c) and (d) M_{TM_AP} (TM = Fe, Co or Ni). In the figure the dashed lines indicate the bias windows.

For the P spin configuration, at zero and low bias voltages, the calculated results show that near the Fermi level the spin-down transport peaks of M_{Fe} and M_{Co} are very low, i.e., $T^{P}_{\downarrow}(E) \ll 1$. As the bias voltage increases, for the two devices some low spin-down peaks gradually enter the bias window, leading to very small $I^{P}_{\downarrow}$. In contrast, the $T^{P}_{\downarrow}(E)$ coefficients of M_{Ni} in the bias window are always very high, indicating some effective transport channels are established in M_{Ni} for the spin-down electrons. These transport channels could effectively transmit the spin-down electrons and result in large $I^{P}_{\downarrow}$. The different transport properties of the systems are mainly attribute to the difference of the chemical bonding

of the molecule and TM chains.

The spin-up coefficients of the three devices for the P spin configurations always approach zero in the bias window ($T^{\mathrm{P}}_{\uparrow}(E) \approx 0$). For example, in the total current of $\mathrm{M_{Ni}}$, the $I^{\mathrm{P}}_{\downarrow}$ component is dominant while the corresponding $I^{\mathrm{P}}_{\uparrow}$ is nearly zero. As a result, the $\mathrm{SFE^P}$ is close to -100% in the whole bias range and $\mathrm{M_{Ni}}$ exhibits very perfect spin-filter capability. As to the AP case, the transmission coefficients of the three devices are always close to zero. There are no noticeable spin-up or spin-down transport channels, even though V_{b} increases from 0 V to 0.5 V. Therefore, the corresponding total current I^{AP} approaches zero and significant GMR effect will appear if the magnetization directions of the electrodes become antiparallel.

In fact, the transport behaviors of the system can be understood from the LDDOS as well. As examples, the zero-bias LDDOSs at Fermi level are depicted in Fig. 6. For $\mathrm{M}_{TM_\mathrm{P}}$, the spin-down components of the LDDOSs of all the devices are delocalized and similar behaviors have also been observed for the finite-bias cases (not shown here). Therefore, the electrons near Fermi level can pass through the devices and form spin-down currents. In contrast, the spin-up LDDOSs of $\mathrm{M}_{TM_\mathrm{P}}$ exhibit quite localized behaviors, indicating that $I^{\mathrm{P}}_{\uparrow}$ should be very small and close to zero. This is consistent with the result of transmission spectra. For the AP spin configuration, the LDDOSs of two spins are both localized, even though V_{b} gradually increases. As a result, there are no transport channels for the AP case and the total current $I^{\mathrm{AP}} \approx 0$ μA.

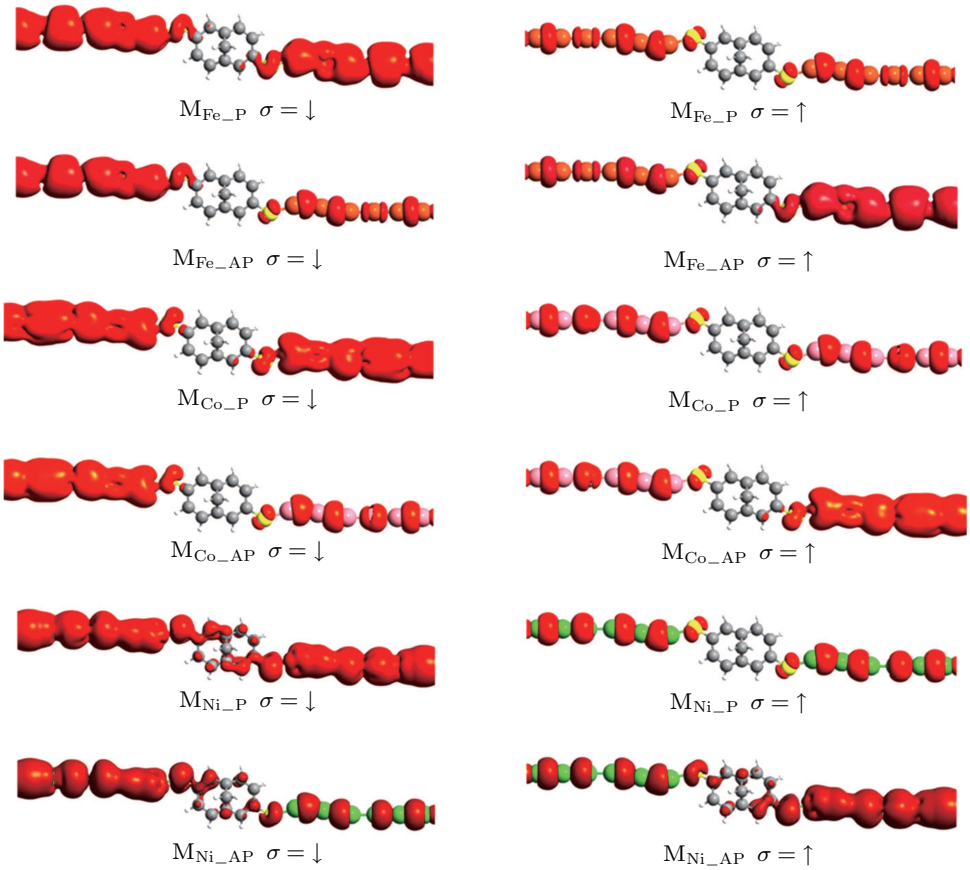


Fig. 6. (color online) The zero-bias LDDOSs at the Fermi level of $\mathrm{M}_{TM_\mathrm{P}}$ and $\mathrm{M}_{TM_\mathrm{AP}}$ (TM = Fe, Co or Ni). The value of the isosurface is 0.005 e/Å^3.

To further elucidate the transport properties of the device, using $\mathrm{M_{Ni}}$ as an example, in Fig. 7 we plotted the spin-down components of the total density of states (TDOS) and the partial density of states (PDOS) of the device. For $\mathrm{M_{Ni_P}}$ and $\mathrm{M_{Ni_AP}}$, the TDOS mainly consists of the p states of the C, S atoms and the d states of the Ni chains, and exhibits similar behaviors. However, the PDOS of $\mathrm{M_{Ni_P}}$ is different from that of $\mathrm{M_{Ni_AP}}$. We see that in the bias window, for the P case, the p states of the molecule and the d states of the two electrodes well hybridize, leading to the formation of delocalized transport channels. In contrast, for the AP case, the d states of the right Ni electrode in the bias window are close to zero. In other words, in the transport process, the contribution from the right electrode can be ignored and there are no effective spin-down transport channels for $\mathrm{M_{Ni_AP}}$, leading to very small current. Therefore, it is not surprising that the GMR effect will appear when the magnetization directions of the electrodes become antiparallel.

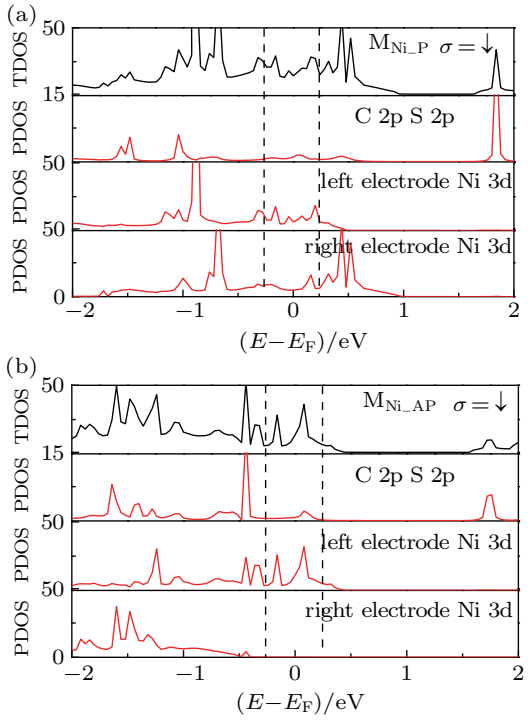


Fig. 7. (color online) The TDOS and PDOS of (a) M_{Ni_P} and (b) M_{Ni_AP} for $V_b = 0.5$ V. The unit is states/eV. In the figure only spin-down components are given and the dashed lines indicate the bias window.

3.2. The spin-polarized optoelectronic properties of M_{Ni} device

Since M_{Ni} has excellent transport properties, finally we investigated the spin-polarized optoelectronic properties. In fact, the optoelectronic properties of various low-dimensional devices have been carefully discussed recently.[46,53,54] However, to our knowledge, the studies on spin-polarized optoelectronic properties of devices are still very limited so far.

It is worth noting that, for the incident light, only monochromatic plane wave was considered. To effectively separate the electron–hole pairs and produce a net photocurrent, a dipole potential is necessary for the photovoltaic process. The dipole potential can be achieved by different methods.[46,53] Like our previous treatment,[53] two small local gate voltages are applied on the electrodes ($V_g = V_{GL} - V_{GR}$, see the inset of Fig. 8). If $V_g \neq 0$ V, an external potential drop is established across the device. Nevertheless, at $z = \pm\infty$, the system is not affected by the local gate voltages and the two electrodes still have the same chemical potentials. As a result, without photons, there is no net current; with photons, electrons may be excited from the occupied states to the unoccupied states and a net photocurrent will be generated by the dipole potential that comes from two gate voltages.

Here we considered two cases, i.e., $V_g = 0.01$ and 0.1 V. The energy range of the incident photons is from 0 eV to 5 eV, including infrared (IR), visible and ultraviolet (UV) light. The calculated spin photoresponse functions R_σ^P and R_σ^{AP} are given in Fig. 8. It is obvious that the characteristic peaks of R_σ^P and R_σ^{AP} curves are different, indicating not only the currents but also the photocurrents are influenced by the magnetization directions of the electrodes. For example, the spin photoresponse functions of the P spin configuration at $V_g = 0.01$ V, R_σ^P, can only be excited by visible and UV light. However in the AP case, non-zero R_σ^{AP} can be generated by IR, visible and UV light.

The spin-polarized photocurrents can be directly excited by the light with given energies and, more importantly, the spin polarization direction of the photocurrent will vary with the incident photon energies. This suggests the device can produce two spin currents by adjusting the photon energies. For example, when $V_g = 0.01$ V and the incident photon energy is about 4.50 eV, in the device the corresponding $R_\downarrow^P$ is about 2.26 a_0^2/photon but $R_\uparrow^P$ is close to zero. As a result, we could obtain very pure light-generated spin-down current. If the photon energy increases to about 4.75 eV, $R_\downarrow^P$ is about zero while $R_\uparrow^P$ become very large, indicating pure spin-up current can also be excited by the light with the given energy.

Furthermore, the direction of photocurrent varies with the photon energy, namely the sign of the photocurrent depends on the parameter. This is particularly important for the AP spin configuration, since in the device the photocurrents with different spins are spatially separated. As can be seen from Fig. 8(b), when the incident photon energy is 3.40 eV, two characteristic peaks are observed for $R_\uparrow^{AP}$ and $R_\downarrow^{AP}$. But the former is positive while the latter is negative. This indicates the spin-up photocurrent appears at right electrode ($+z$) and, at the same time, the spin-down photocurrent appears at the left electrode ($-z$). As a result, the two spin currents can be simultaneously generated and are effectively separated.

Obviously, the microscopic mechanism of spin currents excited by the light is very complicated. Generally speaking, the characteristic peaks at visible and UV ranges may arise from the electron transition between the occupied bands (such as valence band) and the empty bands (such as conduction band). The electron–hole pairs are generated by these high-energy photons and then separated by the external dipole potential. After various spin-dependent scatterings, the carriers finally form spin-polarized photocurrents.

From the microscopic point of view, if the conduction band curvatures are different for $+\boldsymbol{k}$ and $-\boldsymbol{k}$ points ($\boldsymbol{k}$ is the point of Brillouin zone), an imbalanced motion of excited electrons in the conduction bands occurs, which generates a photocurrent in the non-equilibrium situation. Depending on the photon energy, the electrons are activated to different $\boldsymbol{k}$ points in conduction bands and acquire different band velocities. The sign of the photocurrent is determined by the summation of all the activated electrons with different distribution.[54] Therefore, the direction of the photocurrent varies for different photons.

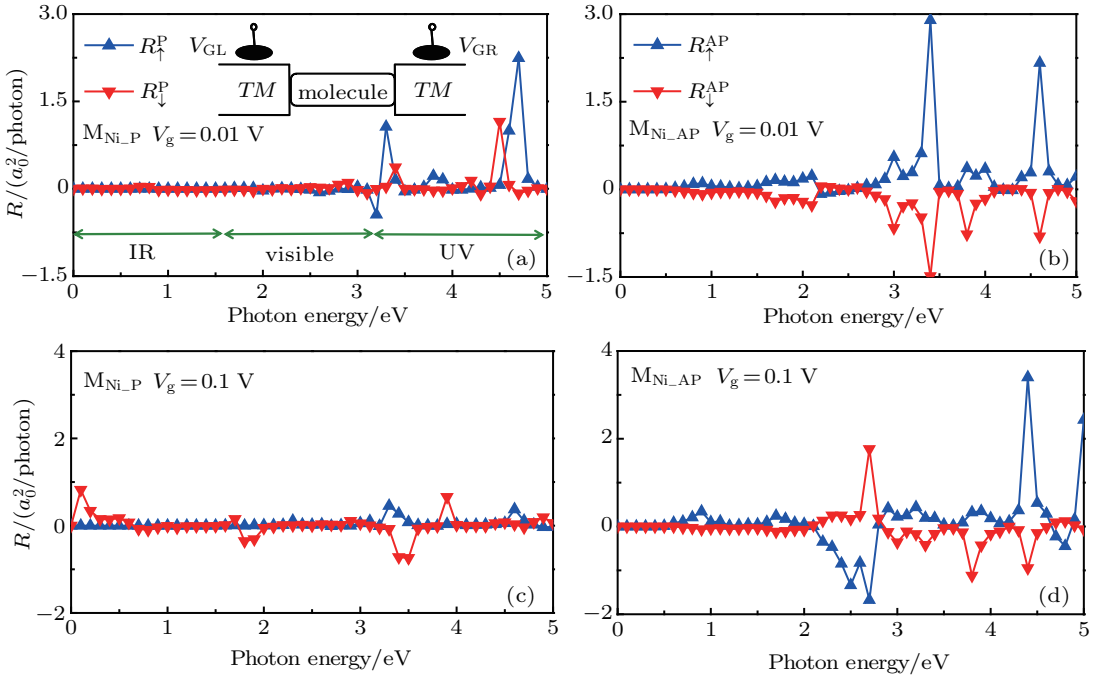


Fig. 8. (color online) (a) and (b) The spin photoresponse functions of M_{Ni} for the P and AP state when $V_g = 0.01$ V. Inset: the schematic structure of the gate-controlled device. (c) and (d) The spin photoresponse functions of M_{Ni} for the P and AP state when $V_g = 0.1$ V. a_0 is the Bohr radius.

When V_g increases to 0.1 V, the R_σ^P and R_σ^{AP} curves change accordingly, indicating we can manipulate the spin photocurrents by V_g as well. We see that the related characteristic peaks exhibit complicated behaviors. A noticeable feature is that, at far IR range, there may exist very low photoresponse peaks (see Fig. 8(c)). We believe the peaks should be attributed to a kind of photon-assisted tunneling (PAT) process, which is a typical quantum effect and has been discussed in our previous study,[53] i.e., with the assistance of low-energy photons, the tunneling probabilities of electrons become larger and the electrons probably form non-zero but very small photocurrents. In other words, the microscopic mechanisms of the photocurrents for low-energy and high-energy photons are different. The PAT effect will provide us with a new way to generate photocurrents with low-energy photons.

4. Conclusions

Using Fe, Co or Ni chains as electrodes, in the present study we systematically investigated the spin-dependent transport properties of the annulene-based molecular spintronic devices. Our results show that these devices could exhibit significant spin-filter effect and have large magnetoresistance. In particular, with Ni chains as electrodes, the device has the best transport properties. In addition, the spin-polarized optoelectronic properties of the device with Ni electrodes are discussed. We found that the spin-polarized photocurrents can be directly generated by irradiating the device with IR, visible or UV light, but the corresponding microscopic mechanisms are different. More importantly, for the AP spin configuration, the photocurrents with different spins are spatially separated, appearing at different electrodes. This phenomenon provides a new way to simultaneously generate two spin currents.

Acknowledgement

The authors give the special thanks to Weixiao Wei for her grammar guidance to the article. She is supported by Soft Science Research Project Research on Propaganda Model of Shanxi Culture Industry (2016041021-2). The authors acknowledge the support from Scientific Cloud Computing Center of Taiyuan University of Technology.

References

[1] Joachim C, Gimzewski J K and Aviram A 2000 *Nature* **408** 541
[2] Flood A, Stoddart J and Steuerman S and Heath J 2004 *Science* **306** 2055
[3] Aviram A and Ratner M A 1974 *Chem. Phys. Lett.* **29** 277
[4] Reed M A 1999 *Proc. IEEE* **87** 652
[5] Liu K, Wang X and Wang F 2008 *ACS Nano* **2** 2315
[6] Javaid S, Bowen M, Boukari S, Joly L, Beaufrand J B, Chen X, Dappe Y J, Scheurer F, Kappler J P, Arabski J, Wulfhekel W, Alouani M and Beaurepaire E 2010 *Phys. Rev. Lett.* **105** 077201
[7] Takács A F, Witt F, Schmaus S, Balashov T, Bowen M, Beaurepaire E and Wulfhekel W 2008 *Phys. Rev. B* **78** 233404
[8] Barraud C, Seneor P, Mattana R, Fusil S, Bouzehouane K, Deranlot C, Graziosi P, Hueso L, Bergenti I, Dediu V, Petroff F and Fert A 2010 *Nat. Phys.* **6** 615
[9] Wende H, Bernien M, Luo J, Sorg C, Ponpandian N, Kurde J, Miguel J, Piantek M, Xu X, Eckhold P, Kuch W, Baberschke K, Panchmatia P M, Sanyal B, Oppeneer P M and Eriksson O 2007 *Nat. Mater.* **6** 516
[10] Mannini M, Pineider F, Sainctavit P, Danieli C, Otero E, Sciancalepore C, Talarico A M, Arrio M, Cornia A, Gatteschi D and Sessoli R 2009 *Nat. Mater.* **8** 194

[11] Yang J F, Zhou L, Han Q and Wang X F 2012 *J. Phys. Chem. C* **116** 19996
[12] Gajek M, Bibes M, Barthélémy A, Bouzehouane K, Fusil S, Varela M, Fontcuberta J and Fert A 2005 *Phys. Rev. B* **72** 020406
[13] Müller M, Luysberg M and Schneider C M 2011 *Appl. Phys. Lett.* **98** 142503
[14] Lee M, Williams J R, Zhang S, Frisbie C D and Gordon D G 2011 *Phys. Rev. Lett.* **107** 256601
[15] Gütlich P and Goodwin H A 2004 *Top. Curr. Chem.* **233** 1
[16] Antonangeli D, Siebert J, Aracne C M, Farber D L, Bosak A, Hoesch M, Krisch M, Ryerson F J, Fiquet G and Badro J 2011 *Science* **331** 64
[17] Lupton J M, McCamey D R and Boehme C 2010 *ChemPhysChem* **11** 304
[18] Wei J H, Liu X J, Xie S J and Yan Y 2009 *J. Chem. Phys.* **131** 064906
[19] Chen B B, Jiang S W, Ding H F, Jiang Z S and Wu D 2014 *Chin. Phys. B* **23** 018104
[20] Urdampilleta M, Klyatskaya S, Cleuziou J P, Ruben M and Wernsdorfer W 2011 *Nat. Mater.* **10** 502
[21] Wu J C, Wang X F, Zhou L, Da H X, Lim K H, Yang S W and Li Z Y 2009 *J. Phys. Chem. C* **113** 7913
[22] Petta J R, Slater S K and Ralph D C 2004 *Phys. Rev. Lett.* **93** 136601
[23] Schmaus S, Bagrets A, Nahas Y, Yamada T K, Bork A, Bowen M, Beaurepaire E, Evers F and Wulfhekel W 2011 *Nat. Nanotechnol.* **6** 185
[24] Matsuura Y 2015 *Chem. Phys. Lett.* **619** 23
[25] Kong X, Cui B, Zhao W, Zhao J, Li D and Liu D 2014 *Org. Electron.* **15** 3674
[26] Pati R, Senapati L, Ajayan P M and Nayak S K 2003 *Phys. Rev. B* **68** 100407
[27] Chen T, Wang L, Li X, Luo K, Xu L, Li Q, Zhang X and Long 2014 *RSC Adv.* **4** 60376
[28] Zhou Y H, Zeng J, Chen K Q 2014 *Carbon* **76** 175
[29] Zheng J, Deng X, Zhao J, Guo P, Guo C, Ren Z and Bai J 2015 *Comput. Mater. Sci.* **99** 203
[30] Li J, Li T, Zhou Y, Wu W, Zhang L and Li H 2016 *Phys. Chem. Chem. Phys.* **18** 28217
[31] Li X, Li H L, Wan H and Zhou G 2015 *Org. Electron.* **19** 26
[32] Bulo R E, Trion L, Ehlers A W, Kanter F J, Schakel M, Lutz M, Spek A L, Lammertsma K 2004 *Chem. Eur. J.* **10** 5332
[33] Choi C H and Kertesz M 1998 *J. Phys. Chem. A* **102** 3429
[34] Dorn H C, Yannoni C S, Limbach H H and Vogel E 1994 *J. Phys. Chem.* **98** 11628
[35] Scott L T and Brunsvold W R 1978 *J. Am. Chem. Soc.* **100** 4320
[36] Barrett D G, Liang G B, McQuade D T, Desper J M, Schladetzky K D and Gellman S H 1994 *J. Am. Chem. Soc.* **116** 10525
[37] Yang X F, Liu Y S, Zhang X, Zhou L P, Wang X F, Chi F, Feng J F 2014 *Phys. Chem. Chem. Phys.* **16** 11349
[38] Caliskan S and Laref A 2014 *Sci. Rep.* **4** 7363
[39] Caliskan S 2013 *Phys. Lett. A* **377** 1766
[40] Brandbyge M, Mozos J L, Ordejon P, Taylor J and Stokbro K 2002 *Phys. Rev. B* **65** 165401
[41] Perdew J P, Burke K and Ernzerhof M 1996 *Phys. Rev. Lett.* **77** 3865
[42] Soler J M, Artacho E, Gale J D, Garcia A, Junquera J, Ordejon P and Portal D S 2002 *J. Phys.: Condens. Matter.* **14** 2745
[43] Svizhenko A, Anantram M P and Govindan T R 2005 *IEEE Trans. Nanotechnol.* **4** 557
[44] Datta S and Houten H V 1996 *Phys. Today* **49** 70
[45] For NanoDcal software, see http://nanoacademic.ca
[46] Chen J, Hu Y and Guo H 2012 *Phys. Rev. B* **85** 155441
[47] Deng X Q, Zhang Z H, Tang G P, Fan Z Q and Yang C H 2014 *Phys. Lett. A* **378** 1540
[48] Zeng J and Chen K Q 2013 *J. Mater. Chem. C* **1** 4014
[49] Zu F X, Liu Z L, Yao K L, Gao G Y, Fu H H, Zhu S C, Ni Y and Peng L 2014 *Sci. Rep.* **4** 4838
[50] Zhao P, Wu Q H, Liu H Y, Liu D S and Chen G 2014 *J. Mater. Chem. C* **2** 6648
[51] Wu Q H, Zhao P, Liu D S, Li S J and Chen G 2014 *Org. Electron.* **15** 3615
[52] Jiang H, Kang D, Xie S and Saxena 2011 *Org. Electron.* **12** 1264
[53] Yang Z, Ji Y L, Lan G, Xu L C, Liu X and Xu B 2015 *Solid State Commun.* **217** 38
[54] Xie Y, Zhang L, Zhu Y, Liu L, Guo H 2015 *Nanotechnology* **26** 455202